Experimental Neurology 267 (2015) 194–208

Contents lists available at ScienceDirect

Experimental Neurology

journal homepage: www.elsevier.com/locate/yexnr

Regular Article

Plasticity of motor network and function in the absence of corticospinal projection

Qi Han [a,1], Changshu Cao [a,b,1], Yuetong Ding [a,1], Kwok-Fai So [a,c,e], Wutian Wu [a,c,e], Yibo Qu [a,*], Libing Zhou [a,b,d,*]

[a] Guangdong–Hongkong–Macau Institute of CNS Regeneration, Jinan University, Guangzhou 510632, PR China
[b] Department of Human Anatomy, Medical School of Jinan University, Guangzhou 510632, PR China
[c] Department of Anatomy, The University of Hong Kong, Pokfulam, Hong Kong SAR, PR China
[d] Co-innovation Center of Neuroregeneration, Nantong University, Jiangsu, PR China
[e] State Key Laboratory of Brain and Cognitive Sciences, The University of Hong Kong, Pokfulam, Hong Kong SAR, PR China

ARTICLE INFO

Article history:
Received 14 December 2014
Revised 9 March 2015
Accepted 10 March 2015
Available online 17 March 2015

Keywords:
Corticospinal tract
Rubrospinal tract
Celsr3
Propriospinal neurons
Motor system

ABSTRACT

Despite the obvious clinical interest, our understanding of how developmental mechanisms are redeployed during degeneration and regeneration after brain and spinal cord injuries remains quite rudimentary. In animal models of spinal cord injury, although spontaneous regeneration of descending axons is limited, compensation by intact corticospinal axons, descending tracts from the brainstem, and local intrinsic spinal networks all contribute to the recovery of motor function. Here, we investigated spontaneous motor compensation and plasticity that occur in the absence of corticospinal tract, using *Celsr3|Emx1* mice in which the corticospinal tract is completely and specifically absent as a consequence of *Celsr3* inactivation in the cortex. Mutant mice had no paresis, but displayed hyperactivity in open-field, and a reduction in skilled movements in food pellet manipulation tests. The number of spinal motoneurons was reduced and their terminal arbors at neuromuscular junctions were atrophic, which was reflected in electromyography deficits. Rubrospinal projections, calretinin-positive propriospinal projections, afferent innervation of motoneurons by calretinin-positive segmental interneurons, and terminal ramifications of monoaminergic projections were significantly increased. Contrary to control animals, mutants also developed a severe and persistent disability of forelimb use following the section of the rubrospinal tract at the C4 spinal level. These observations demonstrate for the first time that the congenital absence of the corticospinal tract induces spontaneous plasticity, both at the level of the motor spinal cord and in descending monoaminergic and rubrospinal projections. Such compensatory mechanisms could be recruited in case of brain or spinal cord lesion or degeneration.

Introduction

Limb movement is driven by spinal motoneurons which receive multiple inputs, including propriospinal, corticospinal, rubrospinal, vestibulospinal, recticulospinal and monoaminergic. The corticospinal tract (CST), in particular, controls fine voluntary movement in rodents through indirect connections with spinal motoneurons, via segmental interneurons (Schieber, 2007). Damage of the CST at the level of the motor cortex or descending tracts occurs in neurological conditions such as spinal cord injury (SCI), amyotrophic lateral sclerosis or cerebral palsy, and is a leading cause of motor disability.

Both in animal models and human disorders, damage of the spinal cord and CST leads to spontaneous reorganization of the motor network and some functional recovery, usually associated with sprouting of spared axons to denervated targets (Nishimura and Isa, 2012; Raineteau and Schwab, 2001; Thuret et al., 2006). For example, following neonatal hemi-decortication or unilateral adult traumatic brain injury, CST fibers originating from the intact hemisphere are able to reach the denervated spinal cord (Ueno et al., 2012; Umeda et al., 2010). In monkeys with C7 spinal cord hemisection, corticospinal descending axons from the intact side cross the midline to innervate the gray matter below the level of the lesion (Rosenzweig et al., 2010). Motor control is also partly restored by a reorganization of spinal intrinsic networks. After the spinal cord section, spontaneous walking recovers, mainly thanks to changes of intrinsic circuitry (Anderson et al., 2007; Bareyre et al., 2004; Courtine et al., 2009; Stelzner et al., 1975; Tillakaratne et al., 2010). Propriospinal neurons, which send axons to different spinal segments (Flynn et al., 2011) and are important for the modulation of

* Corresponding authors at: Guangdong–Hongkong–Macau Institute of CNS Regeneration, Jinan University, Huangpu Avenue West 601, Guangzhou 510632, PR China. Fax: +86 20 85223563.
E-mail addresses: tquyibo@jnu.edu.cn (Y. Qu), tlibingzh@jnu.edu.cn (L. Zhou).
[1] Those authors contributed equally to this work.

http://dx.doi.org/10.1016/j.expneurol.2015.03.008

skilled movements (Azim et al., 2014), can create new intraspinal circuits that bypass injury sites and relay cortical inputs to their original targets (Deng et al., 2013).

The rubrospinal tract (RST) shares many anatomical and functional properties with the CST, such as common segmental interneuron targets in the spinal cord. Both systems may substitute for each other during the execution of skilled movements (Cheney et al., 1991; Kennedy, 1990), and collateral sprouting of one tract could contribute to functional recovery when the other one is injured. Following unilateral lesion of the CST, activity changes in the red nucleus were recorded in the monkey (Belhaj-Saif and Cheney, 2000) and human (Yeo and Jang, 2010). In rats with the section of both CSTs, spontaneous sprouting from the RST was limited, but increased by the administration of neutralizing antibodies against the neurite growth inhibitory protein Nogo-A (Raineteau et al., 2001). Reciprocally, sprouting of the CST did not occur spontaneously following the section of the RST, but could be induced by exogenous neurotrophin-3 (Jeffery and Fitzgerald, 2001). In addition to the CST and RST, other descending pathways such as the reticulospinal, vestibulospinal or tectospinal tracts synapse on spinal segmental interneurons and regulate movement and locomotion (Riddle and Baker, 2010; Soteropoulos et al., 2012), and are also thought to contribute to functional recovery following CST injury (Umeda et al., 2010; Zaaimi et al., 2012).

In lesion models of descending pathways, interpretation of experimental results is difficult because it is nearly impossible to accurately damage a single tract. Here we assessed spontaneous compensation resulting from the specific and genetic deletion of the CST, using *Celsr3|Emx1* mice (Zhou et al., 2008). In these mutant mice, we analyzed motor behavior, anatomical modifications in spinal motoneurons, neuromuscular junctions and spinal segmental interneurons and plasticity of the propriospinal neurons and RST, and tested compensatory roles of the RST in motor control.

Materials and methods

Animals

Animal procedures were performed according to the Guide for the Care and Use of Laboratory Animals of the National Institutes of Health. The protocol was approved by the Laboratory Animal Ethics Committee at Jinan University (Permit Number: 20111008001). Male mice of *Emx1–Cre;Celsr3*$^{+/-}$ genotype were crossed with *Celsr3*$^{f/f}$ females to obtain *Emx1–Cre;Celsr3*$^{f/-}$ mutant mice, named *Celsr3|Emx1* for short, in which *Celsr3* is conditionally inactivated in Emx1 positive cells (Zhou et al., 2008); *Emx1–Cre;Celsr3*$^{f/+}$ or *Celsr3*$^{f/-}$ mice were used as controls. The *Thy1-YFP* transgenic line (Feng et al., 2000) was used to visualize corticospinal axonal projections. Animals of both sexes were used indiscriminately. The numbers of animals used in each experimental set are summarized in Supplementary Table 1.

Behavioral studies

Behavioral tests were carried out by experimenters blind to genotypes. Data were analyzed using EnthoVision XT 7.0 software (Noldus, Netherlands). Open-field tests were carried out as described (Feng et al., 2012). Skilled motor function was assessed by testing food pellet handling. Following deprivation of food and water for 24 h, animals (2–3 months, 25–30 g) were videotaped for food handling. IBB scores ranging from 0 to 9 were used to estimate forelimb usage, based on joint position, object support, digit movement and grasping technique (Irvine et al., 2010).

Walking was assessed using Catwalk™ (Noldus, The Netherlands). Mice walked in an enclosed walkway and images of footprints were recorded. The criteria for data collection were: completing one walk in between 0.5 s and 10 s and walking speed variation less than 60%.

Forelimb recovery after the section of the RST was assessed using rearing and grid tests (Starkey et al., 2005). To measure rearing, mice were placed in a perspex cylinder and videotaped for 5 min. For the grid test, mice explored freely a grid with 2 cm × 2 cm squares for 3 min. Foot slips during the first 50 steps were scored when the paw missed a rung and the animal lost balance, or when the paw slipped off during weight bearing. Mice were tested one day prior to surgery and on the 2nd, 7th, 14th, 28th and 56th day post-surgery.

Surgical procedure for the RST section

Adult mice (2–3 months, 25 − 30 g) were anesthetized with avertin (20 μl/g in distilled water). Under an operating microscope, a dorsal midline incision exposed C4–T2 spines and the longer spine of T2 was used for segment identification. The C4 vertebral lamina on the right side was removed, the dura matter was opened and the lateral one third of the right C4 spinal cord segment was transected with a fine scalpel. After the procedure, animals resumed drinking and eating within 24 h and recovered uneventfully. Mice were allowed to survive for 10 weeks post-surgery.

Histology and immunohistochemistry

For histology, 5 μm thick paraffin sections were stained with 0.1% cresyl violet (Nissl staining) to assess gross morphology. Immunohistochemistry was carried out on 40-μm frozen sections. Rabbit anti-protein kinase Cγ antibody (1:200, ab109539, Abcam) was used to detect the CST in the dorsal funiculus. Goat anti-choline acetyltransferase (1:500, AB144p, Millipore) immunofluorescence was performed to characterize spinal motoneurons. For neuromuscular junction studies, we used rabbit anti-neurofilament 200 (1:1000, N4142, Sigma) to label axon terminal and α-bungarotoxin conjugated to Alexa Fluor 546 (1:1000, T1175, Molecular Probes) to label acetylcholine receptors. Axonal arbors were studied within 50 μm of their distal terminus. Monoclonal antibody to nonphosphorylated neurofilament H (SMI-32, 1:1000, NE1023, Calbiochem) was used to label the red nucleus following FluoroGold tracing. Monoclonal anti-glial fibrillary acidic protein antibody (1:1000, G3893, Sigma) was used to visualize the cut of the RST section. To classify segmental interneurons and propriospinal neurons in the spinal cord, we used the following primary antibodies: rabbit anti-calretinin (1:400, AB5054, Invitrogen), mouse anti-parvalbumin (1:1000, MAB1572, Millipore), rat anti-glycine (1:2000, IG1002, ImmunoSolution), rabbit anti-GABA (1:1000, A2052, sigma), mouse anti-calbindin (1:1000, C9848, Sigma), goat anti-choline acetyltransferase (1:500, AB144P, Millipore). To study monoaminergic neurons and fibers, anti-serotonin (1:1000, S5545, sigma) and tyrosine hydroxylase (1:500, AB152, Millipore) antibodies were used. Signal was detected with a mouse-rabbit ABC kit (PK-6200, Universal, Vector) or with Alexa Fluor 546 or 488 fluorescent secondary antibodies (1:1000, Invitrogen).

Anatomical tracing

Adult mice (2–3 months, 25–30 g) were used for tracing using FluoroGold, wheat germ agglutinin lectin (WGA) and biotinylated dextran amine (BDA). Animals were anesthetized and placed in a head holder (68004, RWD Life Science Co. Ltd, China). For retrograde tracing to the brainstem, 0.6 μl FluoroGold (6% in water; 52-9400, Fluorochrome) was injected in the right side of the C6 segment, and the brains were processed after 3 days. To study propriospinal projections from C3–C4 to the cervical enlargement, we injected 0.5 μl FluoroGold in the right side of the C8–T1 segments, 700 μm lateral to the midline, at a depth of 500 μm, with a glass capillary. After 6–7 days, the brains were fixed and sections at C3–C4 were prepared for immunofluorescence using different markers (indicated above). To study monoaminergic projections, we injected FluoroGold in the C5–C6 segments and prepared sagittal

sections of the brainstem, followed with anti-serotonin and tyrosine hydroxylase immunofluorescence. For retrograde WGA tracing, 5% WGA conjugated to Alexa Fluor 555 (Cat. No. W32464, Invitrogen) was prepared in saline and 1 μl solution was delivered in the upper trunk of the right brachial plexus with a Hamilton syringe. Five days later, samples were prepared and sections of the C5–C6 segments were processed for immunofluorescence using interneuron markers (indicated above).

For anterograde tracing, a 10% solution of BDA (10,000 MW, Molecular Probes) in 0.01 M phosphate buffer (pH 7.4) was injected in the right red nucleus (3.49 mm posterior to the bregma, 0.89 mm lateral to the midline, 3.94 mm ventral to the skull surface). Fourteen days later, animals were anesthetized and perfused with 4% paraformaldehyde. The brains and spinal cords were postfixed overnight at 4 °C. Distribution of BDA was detected in 40 μm thick sections of the cervical spinal cord at C1–C4 by using a nickel-enhanced diaminobenzidine protocol (Sigma).

Pseudorabies virus (PRV) tracing

Transsynaptic connections to motoneurons were studied using PRV-152 (gift from Gary Pickard) which contains a CMV-EGFP reporter gene cassette. Viral recombinants were harvested from pig kidney cell (PK15) cultures, at 1.5×10^9 plaque forming units/ml, and the virus suspension was stored at −80 °C. In postnatal day (P) 21 mice, the right belly of the biceps was exposed through a skin incision under a dissecting microscope, and three injections of 1 μl PRV-152 were administered at three different sites, using a 5-μl Hamilton syringe fitted with a 33-gauge needle. At 48 h, 60 h, 72 h and 96 h post-inoculation, animals were perfused with 0.9% saline followed by 4% paraformaldehyde. Fifty micrometer thick vibratome sections of the C5–C6 segments or brains were prepared and the EGFP signal was captured using a fluorescent or confocal microscope (Leica DM6000B or Zeiss LSM700) equipped with a seamless splicing module.

Cell and fiber counts

To study choline acetyltransferase positive motoneurons in the cervical enlargement, all sections of the C5–C8 segments were grouped into series. Cell number was estimated as the mean of both sides and the mean of one series of choline acetyltransferase-positive cells in the ventral horn was taken as one sample. To analyze FluoroGold-labeled cells in the midbrain and pons, we collected all sections including these regions and counted the number of labeled neurons in every fourth section. To analyze WGA tracing experiments, sections from C5–C6 were divided into series and immunolabeled with antibodies to calretinin, parvalbumin, glycine, GABA, calbindin and choline acetyltransferase. We counted cells positive for tracer, for each interneuron marker, and double-labeled for tracer and marker, in laminae V–VIII. We estimated similarly the number of serotonin and FluoroGold double-labeled neurons in the raphe, and tyrosine hydroxylase and FluoroGold double-labeled cells in the A11 and A13 cell groups.

To assess the density of monoaminergic fibers, stained sections at the C5–C6 segments were scanned at 1 μm interval for stack reconstruction using confocal microscopy (Zeiss LSM700). Fibers were traced and reconstructed using the Imaris FilamentTracer (BitPlane AG, Switzerland) to estimate their density in the intermediate zone (laminae V–VIII) and the ventral horn (laminae IX).

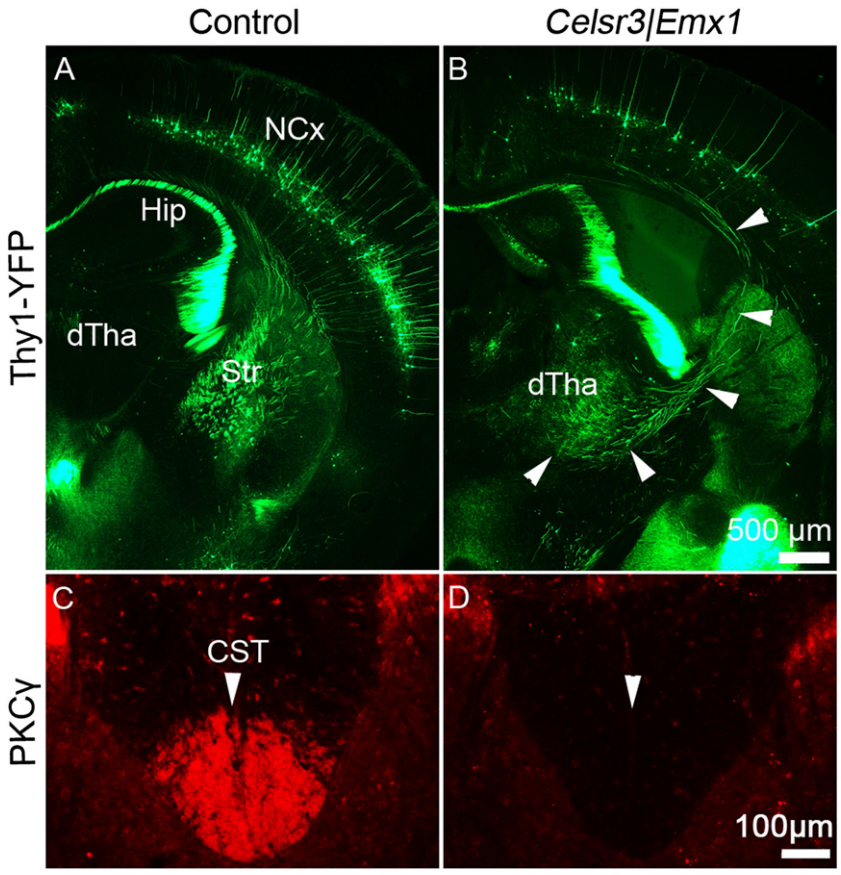

Fig. 1. The CST does not reach the spinal cord in *Celsr3|Emx1* mice. Using the *Thy1-YFP* transgene, pyramidal neurons were labeled in layer V of the neocortex (NCx) and their axons coursed through the striatum (Str) in control mice (A). In *Celsr3|Emx1* mice, the number of Thy1-YFP labeled neurons was reduced and their axons were misrouted to target the dorsal thalamus (dTha) as indicated by arrowheads (B). In transverse sections of the C5–C8 spinal segments, anti-protein kinase Cγ (PKCγ) immunostaining labeled the CST in the dorsal funiculus in control mice but not in the mutant (C, D; arrows). Hip, hippocampus. Five animals were tested in each group.

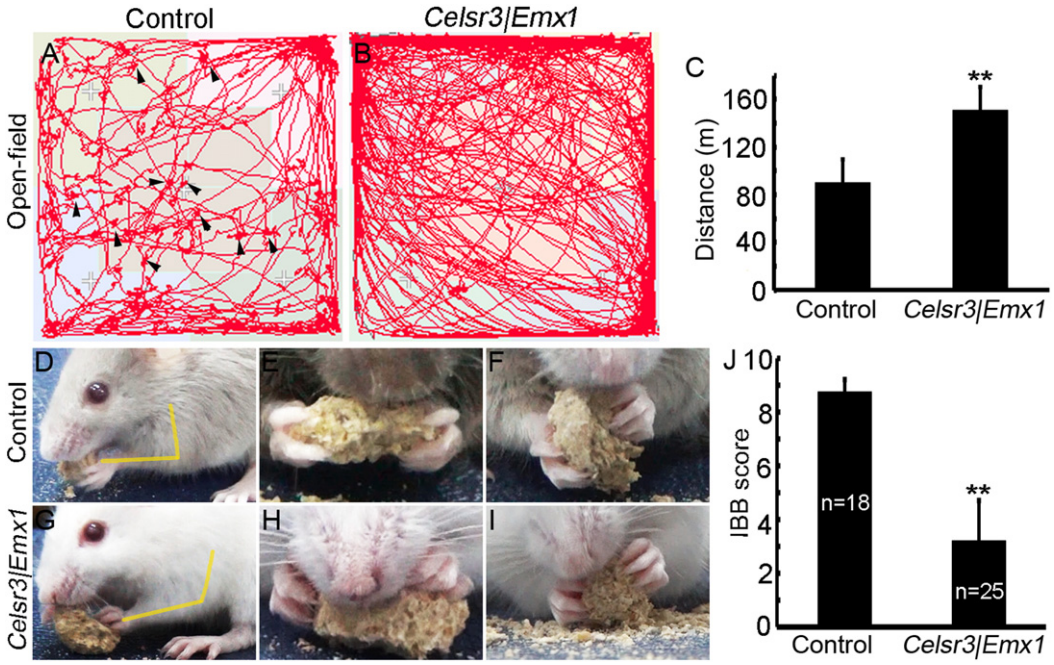

Fig. 2. *Celsr3|Emx1* mice display abnormal motor behavior. In open-field tests, control mice walked with occasional rests (indicated by arrows), and preferred peripheral areas (A), whereas mutant mice moved more and faster, almost without stopping (B). The average distance covered in 30 min was increased in the mutant compared to the control (C, n = 12 in each group). Forelimb skilled movements were assessed by food-taking tests. During eating, the angle of the elbow joint was less than 90° in the control and more than 90° in the mutant (D, G); most control mice (14/18) and few mutant mice (5/25) lifted food pellets from the floor (E, H); control mice could rotate lifted food pellets but mutant mice could not (F, I). The fine movement score IBB was significantly decreased in the mutant compared to the control (J). $^{**}P < 0.01$.

Statistics

Results are expressed as mean ± SEM, and analysis was performed using Student's *t*-test. Statistical significance is expressed as * or **, $P < 0.05$ or $P < 0.01$, respectively.

Results

Celsr3|Emx1 mice are hyperactive and have poor control of fine movements

In *Celsr3|Emx1* mice, corticospinal axons do not grow into the internal capsule and never reach the spinal cord, but thalamocortical reciprocal connections develop almost normally (Zhou et al., 2008). At young adult stages, Thy1-YFP positive corticospinal neurons in layer V are reduced in number, and some mutant Thy1-YFP positive axons are misrouted to the thalamus (Figs. 1A, B; n = 5 in each group). Anti-protein kinase Cγ immunostaining confirmed the presence of the CST in the posterior funiculus of the control but not the mutant spinal cord (Figs. 1C, D; n = 5 in each group). Despite those hodological anomalies, *Celsr3|Emx1* mice grow well, are fertile and behave quite unremarkably, being able to walk, climb, eat, swim and fight.

In the open-field tests, whereas control mice stopped occasionally, *Celsr3|Emx1* mice rarely did, and traveled longer distances than control animals (Figs. 2A–C, $P < 0.01$, n = 12 in each group), suggesting that supranuclear, particularly cortical control, may inhibit spontaneous locomotor activity. Using the Catwalk system to assess voluntary gait (Starkey et al., 2005), we found that print mean intensity, length, width or area, stride length, swing, swing speed, stand and stand index were similar in both genotypes (Supplementary Table 2, n = 16 in each group), confirming that *Celsr3|Emx1* mice have normal walking ability.

The CST is important for the control of fine skilled movement in rodents, primates and humans (Lemon, 2008). To assess skilled movements, we measured the ability to grasp and lift small pellets with the fingers and bring morsels to the mouth. All mice could use both forelimbs to eat. However, whereas almost all control mice (85%, n = 18) lifted pellets from the floor, only 25% of mutant mice (n = 25) did so. To quantify measurements, we used the IBB score described in the Materials and methods section (Irvine et al., 2010). The mean score was 8.8 in the control and 3.2 in the mutant (Figs. 2D–J), demonstrating a diminished ability to manipulate small objects bimanually in *Celsr3|Emx1* mice.

Motor neurons are decreased, and neuromuscular junction function defective in Celsr3|Emx1 mice

The forelimb muscles are controlled by spinal motoneurons in the cervical enlargement. Using Nissl staining, motoneurons in the C5–C8 segments were readily identified due to their large size. They displayed a similar distribution in mutant and control samples, but their number was decreased in the mutant (Figs. 3A, B). Using choline acetyltransferase immunohistochemistry to label motoneurons (Figs. 3C, D), we estimated a 30% reduction of their number in *Celsr3|Emx1* compared to control samples (Fig. 3E; $P < 0.05$, n = 6 in each group). We studied muscle innervation by visualizing post-synaptic acetylcholine receptor clustering using α-bungarotoxin,

Fig. 3. *Celsr3|Emx1* mice have decreased numbers of spinal motoneurons and defective neuromuscular junctions. In coronal sections of the C5–C8 spinal segments, Nissl staining labeled all neurons in the gray matter, and large spinal motoneurons were visible in both the mutant and control ventral horns (A, B). Numbers of choline acetyltransferase (ChAT)-positive motoneurons per section were significantly decreased in the mutant compared to the control (C–E, n = 6). Components of the neuromuscular junction were visualized by anti-neurofilament staining (axonal terminals, green) and α-bungarotoxin staining (acetylcholine receptor clusters, red) in longitudinal sections of the biceps brachii of both genotypes (F, G). Higher magnification of neuromuscular junctions showed that axon terminal arbors were decreased in the mutant compared to the control (H, I), with a significant difference (L). Upon the stimulation of the musculocutaneous nerve, the evoked electromyography potentials were recorded in the biceps. The peak-to-peak electromyography amplitude was decreased in *Celsr3|Emx1* mice compared to control mice (J, K, n = 7 in each group) and the difference was statistically significant (M). C and D are neuromuscular junctions indicated by arrows in A and B, respectively. $^{*}P < 0.05$ and $^{**}P < 0.01$.

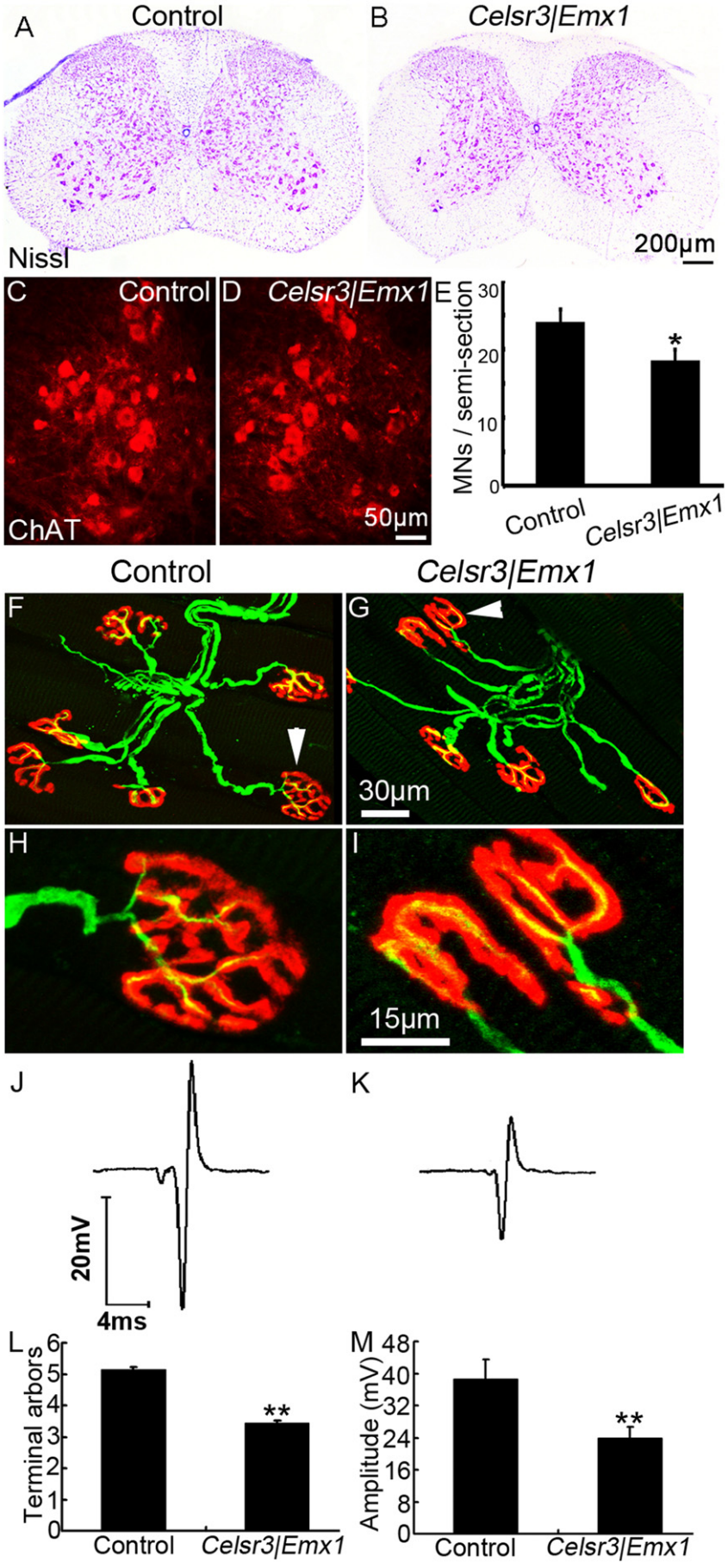
A
Control
B
Celsr3|Emx1
Nissl
200μm
C
Control
D
Celsr3|Emx1
ChAT
50μm
E
MNs / semi-section
30
20
10
0
*
Control
Celsr3|Emx1
Control
Celsr3|Emx1
F
G
30μm
H
I
15μm
J
20mV
4ms
K
L
Terminal arbors
6
5
4
3
2
1
0
**
Control
Celsr3|Emx1
M
Amplitude (mV)
48
40
32
24
16
8
0
**
Control
Celsr3|Emx1

and motor axon terminals using anti-neurofilament immunohistochemistry. Although musculocutaneous nerves innervated the biceps brachii in both genotypes, the terminal axonal arbors were reduced in number and less elaborate in mutants (Figs. 3F–I, L; $P < 0.01$, 40 neuromuscular junctions from 3 animals in each group). To assess whether this atrophy influenced function, we recorded electromyography from the biceps upon the stimulation of musculocutaneous nerves and found that the peak-to-peak amplitude was reduced by 38% in *Celsr3|Emx1* mice compared to controls (Figs. 3J, K, M; $P < 0.01$, n = 7 in each group). This indicates that the reduction of spinal motoneuron number in the ventral horn affects the electrophysiological properties of the biceps. This defect was not strong enough, however, to generate muscle atrophy, since the weight and morphology of the biceps were unaffected in mutant mice (Supplementary Fig. 1).

Afferent innervation of motoneurons by segmental interneurons is altered in Celsr3|Emx1 mice

In rodents, supraspinal inputs are relayed to motoneurons by segmental interneurons (Schieber, 2007). To study interactions between motoneurons and segmental interneurons, we injected a transsynaptic tracer, WGA (Harrison et al., 1984), into the upper trunk (C5–C6) of the brachial plexus (Fig. 4A) and checked the expression of interneuron markers. In transverse sections of the C5–C6 segments, two groups of cells were labeled by WGA on the injection side: motoneurons characterized by large cell bodies in the ventral horn (lamina IX), and smaller interneurons in layers V–VIII (Fig. 4B). The number of interneurons was significantly increased in the mutant (n = 11) compared to the control (n = 16) (119.0 ± 4.20 versus 100.30 ± 3.07 cells per section; $P < 0.01$, Fig. 4C). To determine which interneurons make increased contacts with motoneurons in the mutant, we assessed the expression of the established interneuron markers calretinin, parvalbumin, calbindin, choline acetyltransferase, glycine and GABA. We counted the number of each marker-positive interneurons, and found no difference between genotypes, except for calbindin-positive cells which were slightly less abundant in mutant than in control samples (Fig. 4P), in line with previous reports (Chakrabarty et al., 2009; Han et al., 2013). We then counted each type of interneuron doubly labeled with interneuron markers and WGA (Figs. 4D–O), and normalized to total WGA-labeled interneurons in laminae V–VIII (Fig. 4Q). The ratios were as follows (control versus mutant; n = 6 in each group): calretinin: 29 ± 2% versus 35 ± 1% ($P < 0.05$); parvalbumin: 30 ± 2% versus 25 ± 1% ($P > 0.05$); glycine: 46 ± 1% versus 51 ± 2% ($P > 0.05$); GABA: 4 ± 0.4% versus 3 ± 0.3% ($P > 0.05$); calbindin: 7 ± 0.3% versus: 5 ± 0.2% ($P < 0.01$); and choline acetyltransferase: 1 ± 0.1% versus 1 ± 0.1% ($P > 0.05$). This indicates that calbindin-positive segmental interneurons established less, and calretinin-positive interneurons more contacts with motoneurons in the mutant than in the control cervical enlargement.

Calretinin-positive propriospinal projections are increased in Celsr3|Emx1 mice

Propriospinal neurons connect multiple spinal segments and participate in a variety of functions, such as the modulation of supraspinal descending and afferent sensory inputs (Cowley et al., 2010; Flynn et al., 2011). They play a critical role in motor control and contribute to functional recovery by reorganizing circuits after SCI (Azim et al., 2014; Deng et al., 2013). To study propriospinal neuron projections, we injected FluoroGold in the right spinal segments at C8–T1 and observed labeled propriospinal neurons in C3–C4 (Fig. 5A). Labeled propriospinal neurons were found on both sides, but more on the ipsilateral sides (Fig. 5B). On the contralateral side, the mean number was 40.6 ± 1.9 in the control (n = 12) and 48.4 ± 1.7 in mutants (n = 9), a significant increase (Fig. 5C, $P < 0.01$); no difference was found on the ipsilateral side (not shown). To identify which group of propriospinal neurons increased their projections in the mutant, we studied the expression of interneuron markers in FluoroGold-labeled sections at C3–C4 (Figs. 5D–O). Whereas the number of calretinin-, parvalbumin-, glycine-, GABA-, calbindin- and choline acetyltransferase-positive cells was similar in both genotypes (Fig. 5P; not shown), the number of calretinin- and FluoroGold-labeled neurons was significantly increased in the mutant compared to the control, on both sides (Figs. 5D, E; $P < 0.05$, n = 6 in each group; data not shown). The ratio of calretinin and FluoroGold positive to total FluoroGold-labeled propriospinal neurons on the contralateral side was 18 ± 1% in the control versus 23 ± 3% in the mutant (Fig. 5Q; $P < 0.05$, n = 6 in each group), and 12 ± 1% versus 19 ± 4% on the ipsilateral side ($P < 0.05$, n = 6 in each group). This indicates that calretinin-positive propriospinal neurons in the C3–C4 segments increased their projections to the cervical enlargement in mutant mice.

Rubrospinal projections are increased in Celsr3|Emx1 mice

To examine whether extrapyramidal tracts, such as the RST, vestibulospinal tract and reticulospinal tract, were modified in the absence of the CST, we injected FluoroGold in the C6 spinal segment (Figs. 6A, B) and compared the number of retrogradely labeled neurons in red, vestibular and reticular nuclei. In the midbrain, red nuclei were labeled on the side contralateral to the injection at all rostral–caudal levels (Figs. 6D, E). Labeled neurons in that region were SMI-32 positive, confirming that they corresponded to magnocellular red nuclear neurons (Supplementary Fig. 2). Intriguingly, more red nucleus neurons appeared labeled in mutant than in normal samples (Figs. 6D1–D6, E1–E6). By examining six mice in each group, we estimated that increase to 22% (Fig. 6F). At the pontine level, both vestibular and reticular nuclei were labeled, and their number was similar in both genotypes (Supplementary Fig. 3). This suggests that red nuclei, but not vestibular or reticular nuclei, have more neurons projecting to the spinal cord in response to the congenital absence of the CST.

To study rubrospinal projections further, we injected the anterograde tracer BDA in the red nucleus and analyzed fiber density in the spinal cord (Figs. 6A, C). In transverse sections at C5, highly stained rubrospinal axons were seen in the dorsolateral funiculus contralateral to the injection. Axonal branches could be followed in the gray matter, and some crossed to reach the ipsilateral gray matter, in both genotypes (Figs. 6G, H). In addition, reticulospinal tracts were visible in the anterior funiculus on the ipsilateral side in control and mutant animals, which may be due to the diffusion of BDA beyond the region of the red nucleus (Fig. 6C). The density of rubrospinal axons in the C5 segment was significantly increased on both sides in *Celsr3|Emx1* mutant compared to control mice (Fig. 6I; $P < 0.01$, n = 6 in each group).

Not being transported transsynaptically, FluoroGold and BDA cannot be used to assess whether increased RST projections make connections with motoneurons. To study this, we injected PRV in the biceps and compared the number of transsynaptically labeled neurons (Fig. 7A).

Fig. 4. Calretinin-positive segmental interneurons make increased connections with motoneurons in mutant mice. A: Schematic of WGA injection in the upper trunk of the right brachial plexus to label neurons in the C5–C6 segments. Five days later, WGA labeled motoneurons in the ventral horn and segmental interneurons (INs) were seen in laminae V–VIII on the ipsilateral side (B). The number of WGA-labeled segmental interneurons was significantly increased in the mutant (n = 11) compared to the control (n = 16) (C, *t*-test, $P < 0.01$). WGA-labeled serial sections were labeled with antibodies to calretinin (CR; D, E), parvalbumin (PV; F, G), glycine (H, I), GABA (J, K), calbindin (CB; L, M) and choline acetyltransferase (ChAT; N, O). Double-labeled neurons were indicated by arrows (D–M). The number of different segmental interneurons in laminae V–VIII was comparable in both genotypes, apart from a modest decrease of calbindin-positive segmental interneurons in the mutant (P). The ratio of calretinin and WGA double-labeled segmental interneurons to total WGA-labeled segmental interneurons was significantly increased in the mutant, and the ratio of calbindin and WGA double-labeled segmental interneurons to total WGA-labeled segmental interneurons was significantly decreased, but ratios were unchanged for other interneuron markers (Q). $^{*}P < 0.05$ and $^{**}P < 0.01$; n = 6 for each interneuron marker staining; CC, central canal.

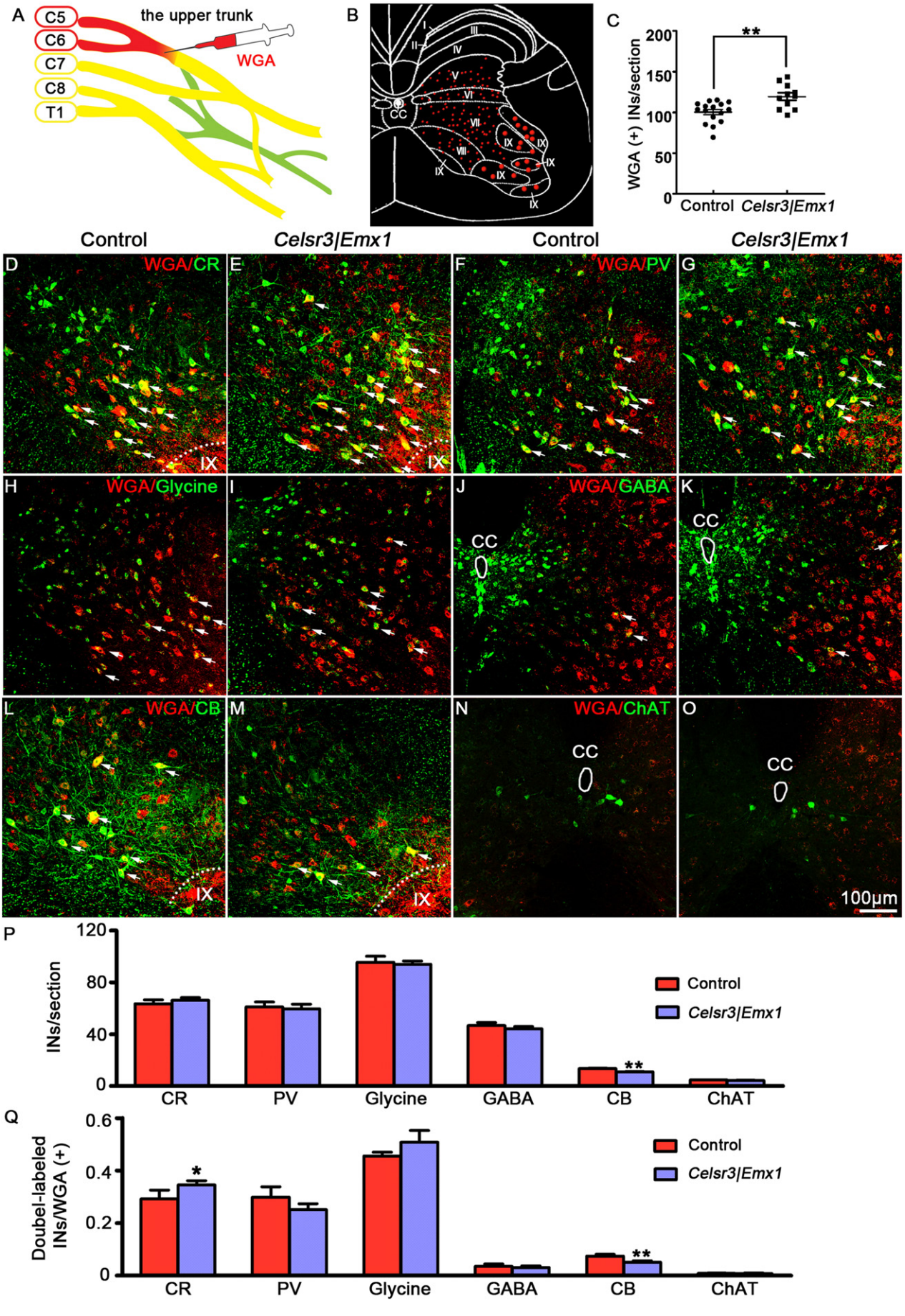
A
C5
C6
C7
C8
T1
the upper trunk
WGA
B
C
WGA (+) INs/section
200
150
100
50
0
**
Control
Celsr3|Emx1
Control
Celsr3|Emx1
Control
Celsr3|Emx1
D WGA/CR
E
F WGA/PV
G
H WGA/Glycine
I
J WGA/GABA
K
L WGA/CB
M
N WGA/ChAT
O
IX
CC
100μm
P
INs/section
120
80
40
0
Control
Celsr3|Emx1
CR
PV
Glycine
GABA
CB
ChAT
Q
Doubel-labeled INs/WGA (+)
0.6
0.4
0.2
0
*
**

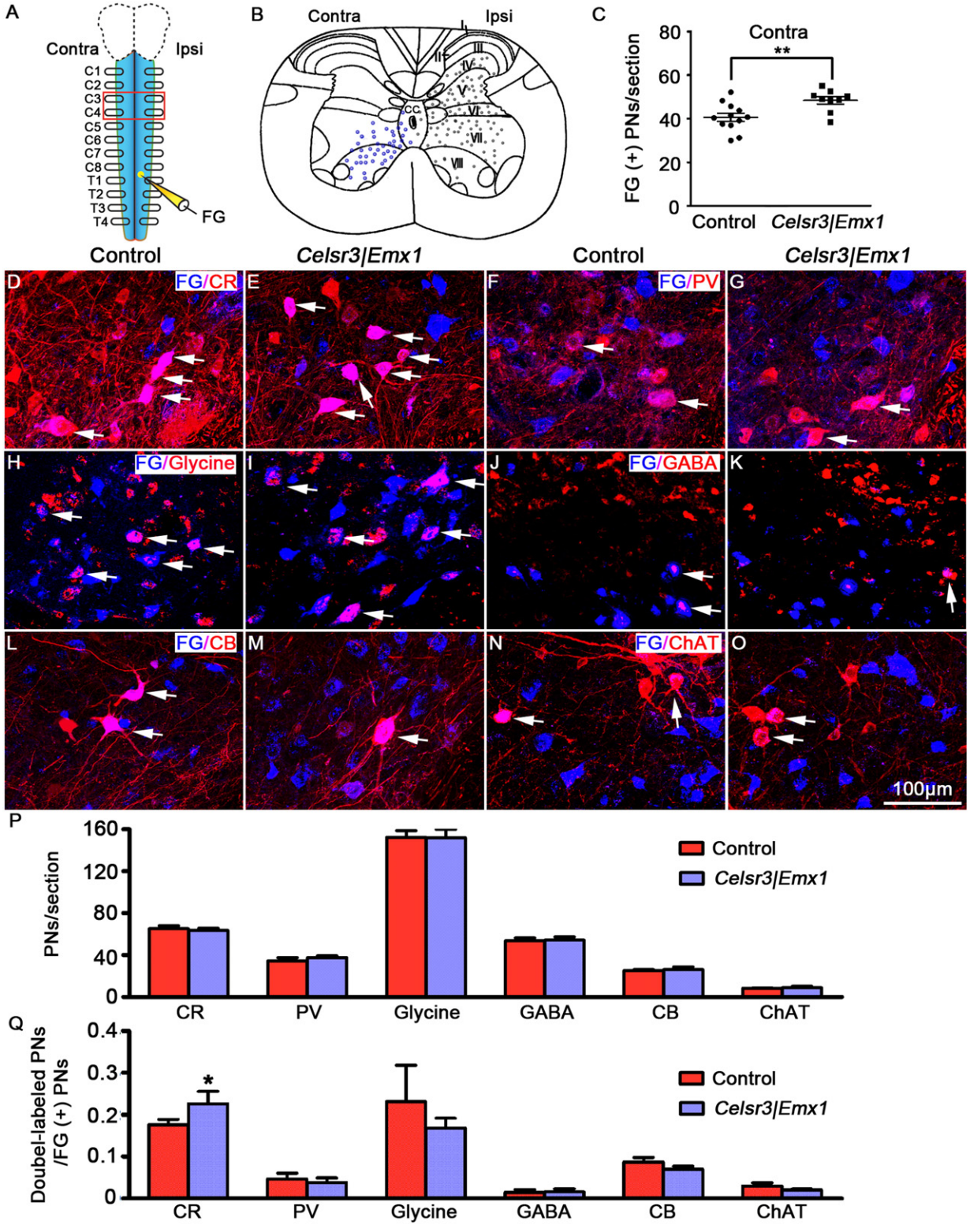

Fig. 5. Calretinin-positive propriospinal neurons at C3–C4 have more contralateral projections to the cervical enlargement in *Celsr3|Emx1* than in control mice. Schema A shows FluoroGold (FG) injection in the right C8–T1 segments and levels of sections studied in the C3–C4 segments. As shown in B, FluoroGold injection resulted in labeled propriospinal neurons (PNs) on both sides, more on the ipsilateral (laminae IV–VIII, gray dots) than the contralateral side (blue dots, mainly in laminae VII and VIII). On the contralateral side, the number of FluoroGold-labeled propriospinal neurons was increased in the mutant (n = 9) compared to the control (n = 12) (C, *t*-test, $P < 0.01$). FluoroGold-labeled sections were stained with antibodies to calretinin (CR; D, E), parvalbumin (PV; F, G), glycine (H, I), GABA (J, K), calbindin (CB; L, M) and choline acetyltransferase (ChAT; N, O). Double-labeled neurons were indicated by arrows (D–O). On the contralateral side, the number of different classes of propriospinal neurons was comparable in both groups (P). The ratio of double labeled calretinin and FluoroGold propriospinal neurons to total FluoroGold-positive propriospinal neurons was significantly increased (Q). $^{*}P < 0.05$; $^{**}P < 0.01$; Contra, contralateral side; Ipsi, ipsilateral side; n = 6 for each interneuron marker staining.

Labeling of different order neurons is time-dependent (Kim et al., 2000; Smeraski et al., 2004). To define the order of connections, we monitored viral labeling at 12 h intervals. After 48 h of the inoculation, ipsilateral motoneurons were retrogradely labeled in the ventral horn (Figs. 7B, C; n = 3 in each group). Abundant ipsilateral labeled segmental interneurons appeared after 60 h, and a few contralateral labeled segmental interneurons were visible 12 h later (Figs. 7D–G; n = 3 in each group). After 96 h, higher order neurons infected by transneuronal passage were clearly identified (Figs. 7H, I). Corticospinal neurons were labeled in the contralateral layer V in control but not in mutant mice (Figs. 7J–M), showing that a 96 h delay is sufficient for PRV propagation to the motor cortex, and therefore enough to label most if not all projections from the brainstem. We counted the number of labeled neurons in red nuclei, reticular nuclei and vestibular nuclei in control (n = 10) and mutant (n = 9) mice in ipsilateral sagittal sections 96 h post-inoculation. The results were as follows (control versus mutant): red nuclei: 538 ± 78 versus 594 ± 83; reticular nuclei: 16768 ± 2800 versus 16576 ± 1672; and vestibular nuclei: 2810 ± 511 versus 3016 ± 276, with no significant difference between genotypes for any nucleus (Fig. 7N). In contrast, on the contralateral side, the number of labeled red nuclei was significantly increased in the mutant (n = 9) compared to the control (n = 10): 1869 ± 119 versus 1502 ± 111 ($P < 0.05$; Fig. 7O), whereas the number of reticular and vestibular nuclei were comparable (respectively 18112 ± 3184 versus 19174 ± 1993, and 3414 ± 537 versus 2752 ± 307) (Fig. 7O). These results suggest that red nuclei, but not vestibular or reticular nuclei, increase their transsynaptic connections with spinal motoneurons in the congenital absence of the CST.

Terminal ramifications of monoaminergic axons are increased in Celsr3|Emx1 mice

Serotonergic and dopaminergic neurons contribute descending projections to all levels of the spinal cord and are implicated in the initiation of locomotion (Jordan et al., 2008; Liu and Jordan, 2005; Musienko et al., 2011). Spinal projecting serotoninergic neurons are located mainly in the B1 – B3 parapyramidal raphe areas (Jones and Light, 1992; Jordan et al., 2008) (Supplementary Fig. 4A), whereas spinal projecting dopaminergic neurons are primarily found in the hypothalamic A11 region (Qu et al., 2006; Skagerberg and Lindvall, 1985) (Supplementary Fig. 4B). To investigate plastic changes of monoaminergic innervation, we used anti-serotonin and anti-tyrosine hydroxylase immunofluorescence of the C5 – C6 sections traced by WGA injection in the brachial plexus. Highly stained serotonin-positive fibers were widely spread in the intermediate zone (laminae V–VIII) and the ventral horn. Some fibers came in close contact with WGA-labeled segmental interneurons in the intermediate zone and with motoneurons in the ventral horn (Figs. 8A, C, E, G). We estimated fiber density using tri-dimensional reconstruction and found it increased in both regions in the mutant compared to the control (Figs. 8B, D, F, H, Q, R; $P < 0.01$, n = 6 in each group). Tyrosine hydroxylase-positive fibers were visible in the intermediate zone, and some appeared to contact WGA-labeled segmental interneurons (Figs. 8I, K). In the ventral horn, they were abundant and some seemed to contact WGA-labeled motoneurons, particularly in the mutant (Figs. 8M, O). Their number was significantly increased in both regions in the mutant relatively to the control (Figs. 8J, L, N, P, Q, R; $P < 0.01$, n = 6 in each group). Increased monoaminergic fiber density

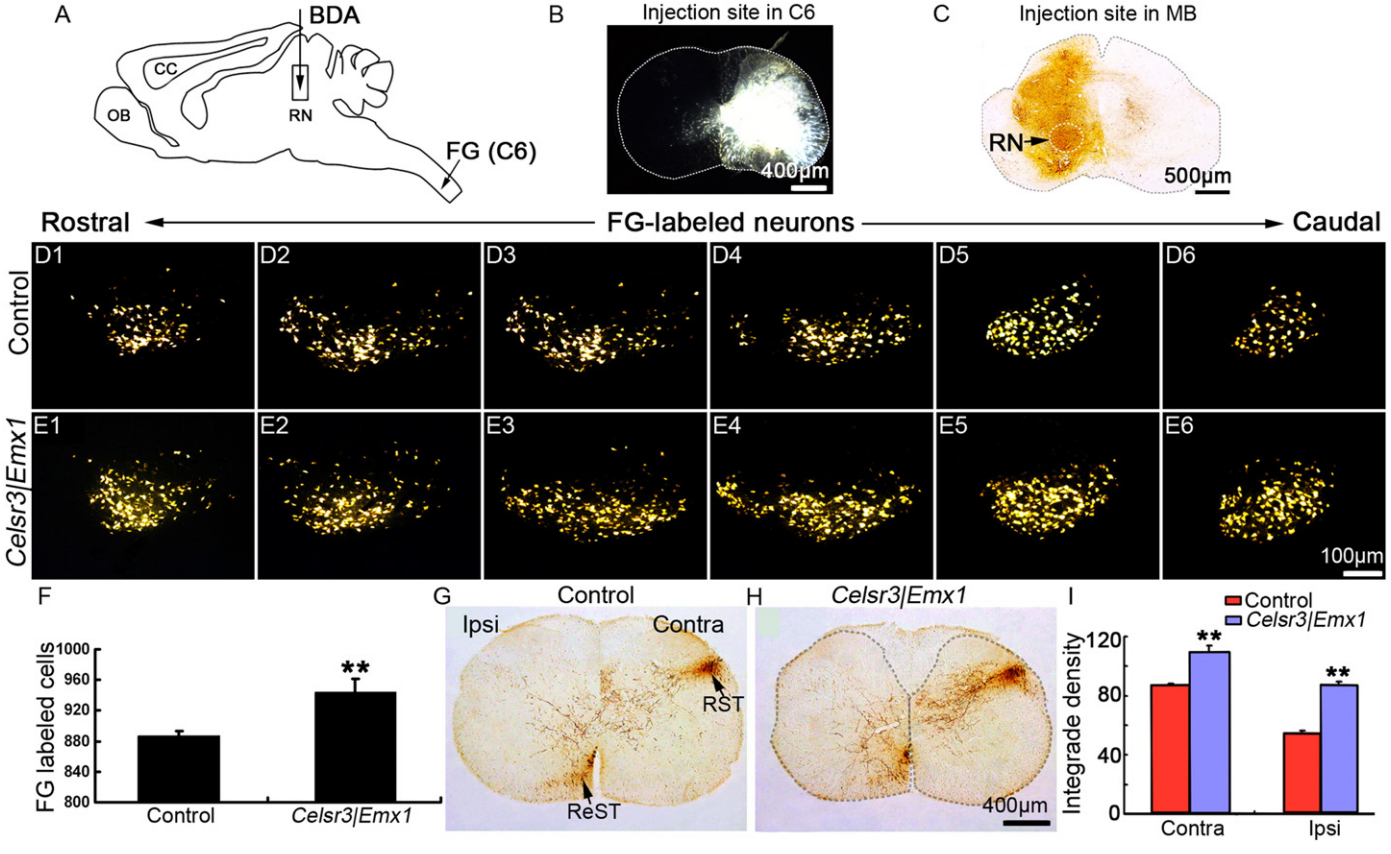

Fig. 6. Projections of red nuclei to the spinal cord are increased in *Celsr3|Emx1* mice. Schema A illustrates the injection of FluoroGold (FG) to the C6 segment, and of BDA in the red nucleus (RN). The FluoroGold injection site was identified in transverse sections of the C6 segment (B), and the BDA injection site was visible in coronal sections of the midbrain (MB), with diffusion to reticular formation (C). More retrogradely FluoroGold-labeled neurons were counted on the left side of the midbrain in mutant than in control samples (D1–D6, E1–E6), as shown in F (FluoroGold positive cells/section). Upon BDA midbrain injection, in the C5 segment, positive rubrospinal and reticulospinal fibers were present on the contralateral and ipsilateral sides, respectively, and some axonal branches were visible in the gray matter on both sides in both genotypes (G, H). Fiber density on contralateral (Contra) and ipsilateral (Ipsi) sides was significantly increased in *Celsr3|Emx1* mice compared to the control (I). **t-Test, $P < 0.01$, n = 6; OB, olfactory bulb; cc, corpus callosum.

in mutants could result from more monoaminergic neurons sending axons to the spinal cord, increased axonal ramification, or both. To assess this, we estimated the number of monoaminergic projecting neurons by injecting FluoroGold in the left gray matter of the C5–C6 segments, followed with anti-serotonin and anti-tyrosine hydroxylase immunofluorescence. The number of serotonin-positive neurons in the raphe was comparable in both groups (not shown). Most serotonin and FluoroGold double-labeled neurons were present in the B3 area (Supplementary Figs. 4C, E), where their number was similar in mutant and control mice (Supplementary Fig. 4G). The number of tyrosine

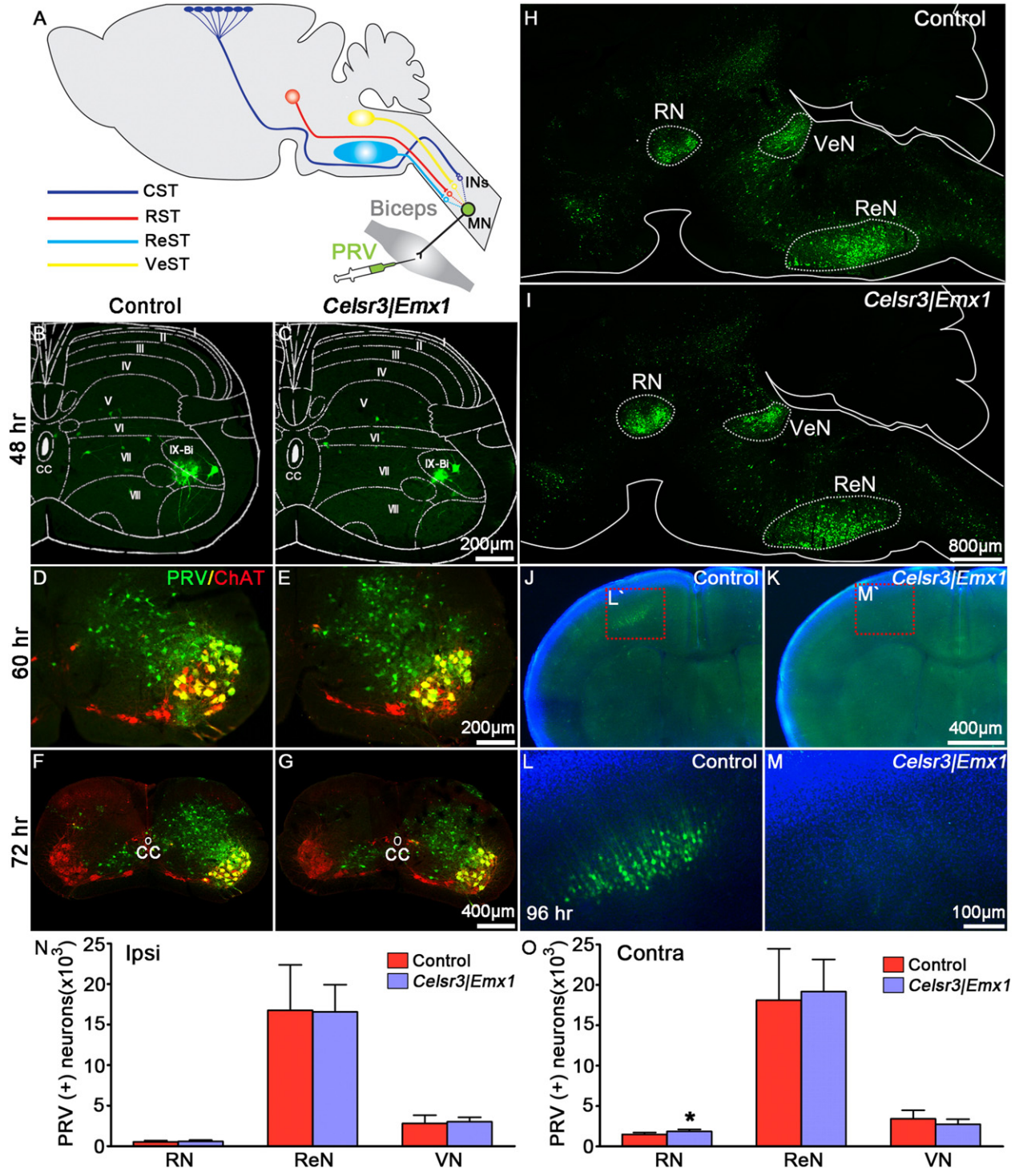

Fig. 7. Transsynaptic connections between red nuclei and motoneurons are increased in *Celsr3|Emx1* mice. Schema A shows PRV injection in the biceps, with transsynaptic labeling of different supraspinal tracts, including the CST (blue), RST (red), vestibulospinal tract (VeST, yellow) and reticulospinal tract (ReST, light blue). PRV mainly labeled motoneurons in the ventral horn in both genotypes 48 h after inoculation (B, C, n = 3). In addition to choline acetyltransferase (ChAT, red) positive motoneurons, many ipsilateral segmental interneurons (green) were traced 60 h post-inoculation (D, E, n = 3), and contralateral segmental interneurons were also visible 12 h later (F, G, n = 3). After 96 h, red nuclei (RN), vestibular nuclei (VeN) and reticular nuclei (ReN) were labeled in both genotypes (H, I), and corticospinal neurons were labeled in the control (J, L) but not in the mutant (K, M). The number of neurons in the red nucleus contralateral to virus injection was significantly increased in the mutant (n = 9) compared to the control (n = 10) ($P < 0.05$), but the numbers of neurons in vestibular nuclei and reticular nuclei were comparable in both groups (O). On the ipsilateral side, no significant difference between control and mutant mice was found (N). L′ and M′ are higher magnification of boxed areas in J and K, respectively. *$P < 0.05$.

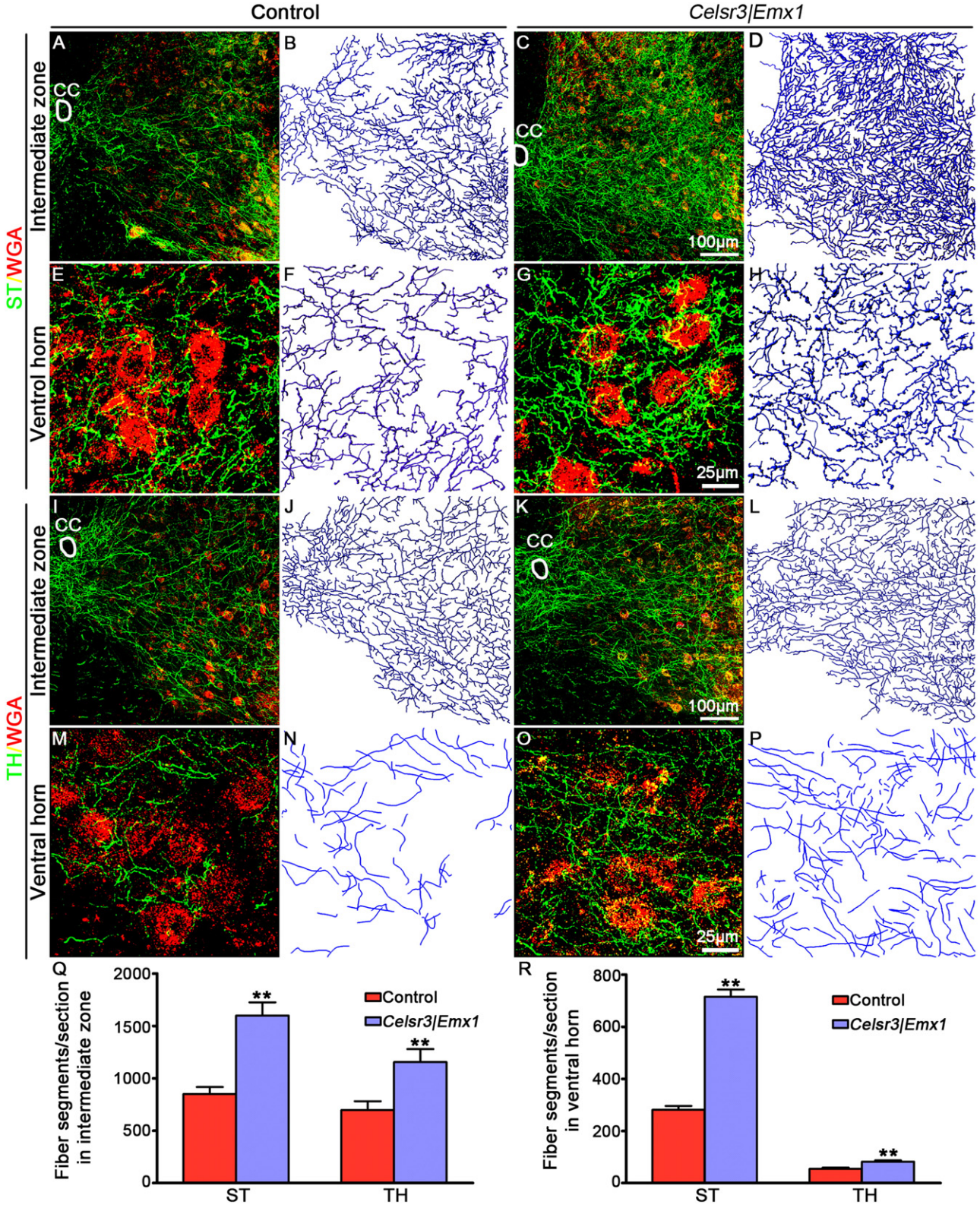

Fig. 8. *Celsr3|Emx1* mice have more monoaminergic fibers in the spinal cord than control mice. WGA-labeled sections of the C5–C6 segments were stained with anti-serotonin (ST) and anti-tyrosine hydroxylase (TH) antibodies. In control (A, B) and mutant (C, D) mice, ST-positive fibers were dispersed in the intermediate zone, intermingled with WGA-labeled segmental interneurons (A, C); in the ventral horn, some made close contacts with WGA-labeled motoneurons (E, G). Using tri-dimensional reconstruction, fiber density in the intermediate zone (B, D) and the ventral horn (F, H) was increased in the mutant (D, H, n = 6) compared to the control (B, F, n = 6). TH-positive fibers showed similar distribution patterns as ST-positive fibers in the intermediate zone (I, K) and the ventral horn (M, O). The fiber density in both regions was increased in the mutant (L, P, n = 6) compared to the control (J, N, n = 6). ST- and TH-positive fibers were significantly increased in the mutant intermediate zone (Q) and ventral horn (R) (*t*-test, $P < 0.01$, n = 6). $^{**}P < 0.01$; CC, central canal.

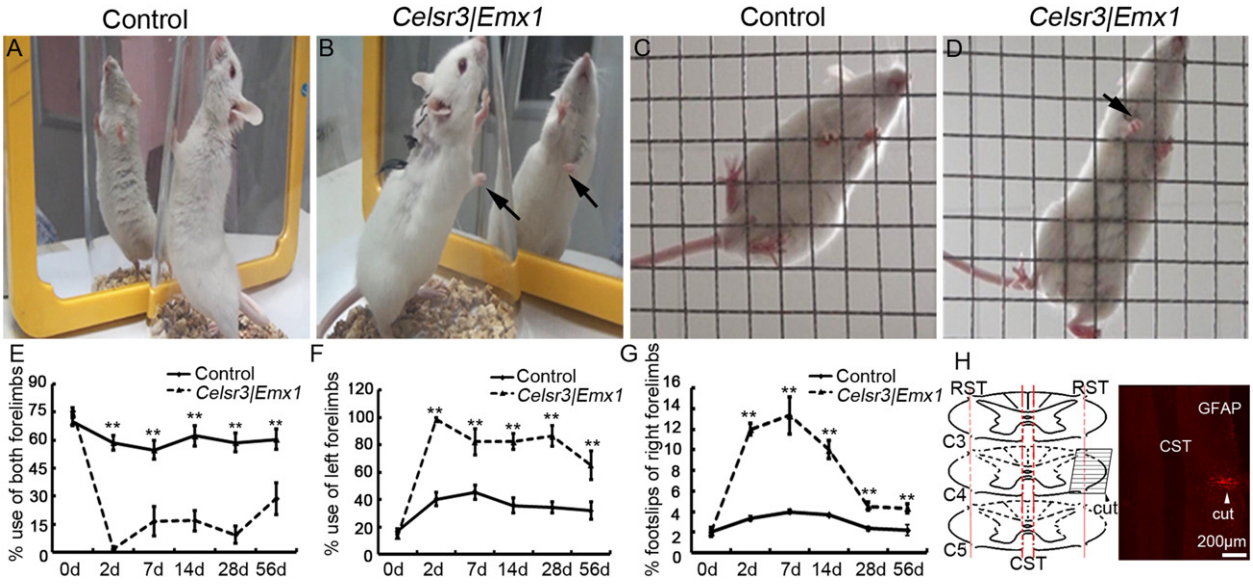

Fig. 9. Following the section of RST, *Celsr3|Emx1* mice do not recover the use of the forelimbs. After the C4 right lateral spinal section, the use of the forelimbs was assessed using the rearing test. On the 7th day after surgery, control mice could use both forelimbs (A) whereas mutant mice could not use the right forelimb (B, arrows). Forelimb use was measured prior to surgery and on the 2nd, 7th, 14th, 28th, and 56th day after surgery. Before surgery, both groups of mice used both forelimbs indiscriminately. After surgery, the use of both forelimbs was decreased in *Celsr3|Emx1* mice but not in control mice (E), and the use of the single left forelimb was increased in the mutant compared to the control (F). Forelimb function was further assessed using foot slip tests. Prior to surgery, no differences related to genotypes were noted. Control mice accurately placed the right forepaw on the rung of an elevated grid (C), whereas mutant mice failed quite often (D, arrow). Errors were dramatically increased in the mutant compared to the control on the 2nd, 7th, 14th, 28th, and 56th day after surgery (G). H illustrates one section of about one third of a lateral C4 spinal section including the RST (left panel); the location of the cutting site was validated by anti-glial fibrillary acidic protein (GFAP) immunofluorescence (right panel). $^{**}P < 0.01$; n = 6 in each group.

hydroxylase-positive neurons in areas A11 and A13 was also not significantly different in control and mutant samples (not shown). Most tyrosine hydroxylase and FluoroGold double-labeled neurons were located in the A11 group (Supplementary Figs. 4D, F), in similar number in both genotypes (Supplementary Fig. 4G). This suggests that the terminal ramifications of monoaminergic axons, rather than the number of monoaminergic neurons, are increased in the *Celsr3|Emx1* spinal cord.

Celsr3|Emx1 mice recover poorer than control mice following the section of the RST

As the CST and the RST work in synergy in motor control (Cheney et al., 1991), we wondered whether the increased projection from the RST could palliate the lack of cortical projections in *Celsr3|Emx1* mice. If this is the case, sectioning the RST should result in more severe deficits in mutant than in control mice. We sectioned the lateral tier of the right spinal cord at C4 in normal and mutant animals (Fig. 9H, n = 6 in each group), and tested right forelimb function on the 2nd, 7th, 14th, 28th and 56th day post-surgery, using the rearing test (Figs. 9A, B). Before surgery, animals of both genotypes displayed similar ability to use both forelimbs (70% in controls versus 75 % in mutants, n = 6 in each group, $P > 0.05$; single left forelimb usage 16% in controls versus 13% in mutants, $P > 0.05$). After surgery, all mice had obvious right forelimb paresis, but control mice recovered rapidly, back to pre-surgery levels within two days. In the mutant, the use of right forelimbs on the injured side was reduced and that of the left forelimbs was significantly increased at the different time points after surgery, compared to control mice (Figs. 9E, F). There was a subtle recovery of forelimb use on the injured side in mutants, since forelimb use reached 29% on the 56th day versus 17% on 7th day, but this was not significant. We compared the foot slip using grid tests (Figs. 9C, D). As shown in Fig. 9G, the percentage of right forelimb foot slips was significantly increased in mutant versus control mice, although errors decreased gradually and reached a stable value (4%) on the 28th day post-surgery, indicating that mutants remained able to learn motor skills.

Altogether, these results show that, following the RST section, the function of the ipsilateral forelimb is defective and recovers minimally in *Celsr3|Emx1* mice, whereas control mice recover rapidly and fully.

Discussion

Using *Celsr3|Emx1* mice in which the CST is specifically and fully absent, we confirm the importance of the CST for fine skilled movements in rodents. We show that the absence of the CST results in hyperactive behavior with decreased numbers of motoneurons and neuromuscular junctions. CST-defective spinal cords have increased calretinin-positive propriospinal neuron projections and monoaminergic terminal arborizations, and more interactions of calretinin segmental interneurons with motoneurons. The absence of the CST results in increased size of red nuclei and the RST, but does not affect the vestibulospinal tract or reticulospinal tract. Furthermore, it hampers severely functional recovery following the section of the RST.

Celsr3|Emx1 mice provide a novel model of motor plasticity in the absence of the CST

Celsr3 is required for the development of many axonal tracts (Tissir et al., 2005; Tissir and Goffinet, 2013). In *Celsr3|Emx1* mice, *Celsr3* is inactivated specifically in cortical projection neurons, resulting in the complete absence of corticospinal projections and postnatal death of layer V neurons. Intriguingly, some mutant layer V axons normally destined to the hindbrain or spinal cord are misrouted to the thalamus, perhaps by following corticothalamic axons that are preserved by the mutation. Using PRV tracing, we did not find any labeled neuron in mutant layer V, confirming that no mutant corticospinal axons reached the spinal cord. Although the CST is affected in other mutant mice (Cohen et al., 1998; Greig et al., 2013; Liu et al., 1993, 2005; Ozdinler and Macklis, 2006), as far as we know, none of them combines a complete and specific absence of the CST with a normal survival and healthy status compatible with experimental investigation. Other mouse models have been described in which the CST is destroyed or corticospinal projection neurons are severed (Terashima, 1995). It is not possible to

experimentally damage the CST with the specificity and precision afforded by genetic models. On the other hand, the genetic absence of the CST from the onset of development may not model faithfully the reaction of the motor system that is triggered by its lesion.

Although the CST is indispensable for skilled motor function in humans and monkeys, its role in other species and particularly rodents is debated. Cats in which the cerebral cortex is surgically removed around birth can acquire skills such as eating, drinking, grooming and even learning (Bjursten et al., 1976). In line with other models such as rats with a unilateral CST transaction, which show a prompt recovery of symmetric locomotion (Muir and Whishaw, 1999), we found that *Celsr3|Emx1* mice had no defect in gross postural movements and gait. In contrast, skilled finger movements were drastically affected. Mutant mice did rarely lift food pellets from the floor and had poor bimanual scores. This shows that the CST is required for hand dexterity and fine movement in rodents, like in cats and primates (Alstermark et al., 1981; Lawrence and Kuypers, 1968).

Another prominent trait in *Celsr3|Emx1* mutants is their increased spontaneous locomotor activity. The result is similar to that reported in rats, in which decortication led to increased activity in running wheels (Kolb and Whishaw, 1981). Studies in rodent SCI models suggest that segmental interneurons that relay descending signals provide rhythmic inhibitory input to motoneurons, and are themselves inhibited by the CST (Wilson et al., 2010). The hyperactivity observed in *Celsr3|Emx1* mice may thus reflect a decreased inhibitory action of segmental interneurons on spinal motoneurons. In our study, approximately 30% segmental interneurons and 20% intersegmental propriospinal neurons were positive for calretinin, and both contingents were increased in mutant spinal cord. The presence of calretinin-positive neurons with large cell bodies and prominent dendrites in laminae V–VI and VII–VIII is well known (Alvarez et al., 2005; Antal et al., 1990; Liu et al., 2010; Ren and Ruda, 1994), but their role in movement control is not fully understood. Our results suggest that calretinin-positive segmental interneurons and/or propriospinal neurons may contribute to remodeling spinal motor circuits, leading to spontaneous hyperactivity. Electrophysiological studies in vivo are required to demonstrate this directly.

The observed increase in serotonin and dopamine spinal innervation in *Celsr3|Emx1* mutants could also contribute to the modification of motor behavior. Serotonin projections from parapyramidal raphe nuclei are known to facilitate the initiation of movements (Jones and Light, 1992; Jordan et al., 2008; Liu and Jordan, 2005). In the spinal cord, serotoninergic fibers can activate central pattern generators that produce rhythmic outputs, even after the loss of the CST (Harris-Warrick and Cohen, 1985; Schmidt and Jordan, 2000). Similarly, dopaminergic neurons, particularly from the A11 diencephalic group, send axons to the spinal cord to modulate locomotor function (Barriere et al., 2004; Clemens et al., 2012; Han et al., 2007).

The RST palliates defective CST function

In *Celsr3|Emx1* mice, axonal projections from red nuclei to the spinal cord are increased, and experimental section of the RST leads to defective forelimb use, with almost no recovery. In contrast, the section of the RST in normal mice results in partial motor deficits that recover rapidly. Thus, in the mutant, the RST palliates defective CST function in movement control. Other extrapyramidal tracts, such as the reticulospinal tract and the vestibulospinal tract, were also damaged during surgical procedure, and the reticulospinal system might also mediate some functional recovery following corticospinal lesions (Umeda et al., 2010; Zaaimi et al., 2012). However, we did not find changes of spinal projections from vestibular nuclei or the reticular formation, which leads us to believe that the main plasticity in our model is due to the RST. In patients with CST injuries, neuronal activity of red nuclei was elevated (Yeo and Jang, 2010), and the reorganization of rubrospinal output after unilateral CST lesion was demonstrated in monkeys (Belhaj-Saif and Cheney, 2000). Those observations suggest that promoting RST function may help recovery following CST lesions. Furthermore, the observation that red nuclei are increased in size when the CST is absent suggests that the RST and CST may compete for common spinal targets and/or growth factors during development. In addition, the plasticity of increased monoaminergic projections and afferent innervations by calretinin-positive spinal neurons may also contribute to motor control, which should be studied further.

The Celsr3|Emx1 mouse model is clinically relevant

Our model is pertinent to studies of prenatal brain injury, amyotrophic lateral sclerosis, and to a lesser extent traumatic SCI. Prenatal CST injury is a major determinant of motor impairment in cerebral palsy patients, and abnormalities of the CST measured by imaging are significantly correlated with motor function in children with cerebral palsy (Krageloh-Mann and Horber, 2007; Woodward et al., 2006; Yoshida et al., 2010). In that disorder, lesions of the CST occur during fetal development. Our genetic model may be more appropriate than investigations using postnatal lesions of the motor cortex or CST.

Amyotrophic lateral sclerosis is characterized by the degeneration of upper and lower motoneurons (Jackson and Bryan, 1998). Although the loss of spinal motoneurons is a key determinant of clinical diagnosis and symptoms (Ferguson and Elman, 2007), the decreased size of the CST measured with MRI is a useful disease index, correlated with disease severity, and differentiating it from progressive muscular atrophy (Cosottini et al., 2005). Despite significant progress, the cause of motor neuron death in amyotrophic lateral sclerosis remains unexplained (Andersen and Al-Chalabi, 2011). In particular, whether upper motor neuron impairment contributes to the degeneration of lower motoneurons remains controversial (de Carvalho et al., 2011). *Celsr3|Emx1* mice display a combination of upper cortical and lower spinal motoneuron loss. As *Celsr3* inactivation in the neocortex does not affect the spinal cord directly, lower motoneuron loss is likely secondary to the absence of the CST. Our previous studies indicate that the maturation and regeneration of spinal cord motoneurons are dependent on cortical inputs (Ding et al., 2014; Han et al., 2013), and the present results support the notion that the impairment of the CST in amyotrophic lateral sclerosis affects the survival of lower motoneurons. Whether CST innervation affects spinal motoneurons via some neurotrophic factors or by regulation of neural activity is unknown. In amyotrophic lateral sclerosis spinal cord, levels of ciliary neurotrophic factor and nerve growth factor are significantly decreased (Anand et al., 1995), but it is unclear whether these changes are due to impairment of CST projections. Differential screening of gene and protein expression in *Celsr3|Emx1* and control spinal cord may help clarify that question.

Spinal cord injury is a leading cause of motor disabilities for which our therapeutic arsenal remains limited (Thuret et al., 2006). It is often considered that plasticity developmental mechanisms could be redeployed during regeneration. Even though the genetic absence of the CST does not accurately model CST injury, our mutant mice could prove useful to test different therapeutic measures aiming to foster spinal cord motor recovery after injury.

Conflict of interest

The authors declare no competing financial interests.

Acknowledgments

We wish to thank Kevin Jones for *Emx1–Cre* mice, Fadel Tissir for *Celsr3* mutant mice, Yiwen Ruan for discussion and techniques, and Pickard E. Gary for providing PRV. This work was supported by grants from the National Natural Science Foundation of China (81171152 and 31070955, L. Zhou), National Basic Research Program of China (973 Program, 2011CB504402 to L. Zhou and 2014CB542205 to Y. Qu.), Foundation for High-level Talents in Higher Education of Guangdong

(50524005), Project of Internation as well as Hong Kong, Macao & Taiwan Science and Technology Cooperation Innovation Platform in Universities in Guangdong Province (2013gjhz0002), Programme of Introducing Talents of Disciplineto Universities (B14036), and Fundamental Research Funds for the Central Universities (21614603).

Appendix A. Supplementary data

Supplementary data to this article can be found online at http://dx.doi.org/10.1016/j.expneurol.2015.03.008.

References

Alstermark, B., Lundberg, A., Norrsell, U., Sybirska, E., 1981. Integration in descending motor pathways controlling the forelimb in the cat. 9. Differential behavioural defects after spinal cord lesions interrupting defined pathways from higher centres to motoneurones. Exp. Brain Res. 42, 299–318.

Alvarez, F.J., Jonas, P.C., Sapir, T., Hartley, R., Berrocal, M.C., Geiman, E.J., Todd, A.J., Goulding, M., 2005. Postnatal phenotype and localization of spinal cord V1 derived interneurons. J. Comp. Neurol. 493, 177–192.

Anand, P., Parrett, A., Martin, J., Zeman, S., Foley, P., Swash, M., Leigh, P.N., Cedarbaum, J.M., Lindsay, R.M., Williams-Chestnut, R.E., et al., 1995. Regional changes of ciliary neurotrophic factor and nerve growth factor levels in post mortem spinal cord and cerebral cortex from patients with motor disease. Nat. Med. 1, 168–172.

Andersen, P.M., Al-Chalabi, A., 2011. Clinical genetics of amyotrophic lateral sclerosis: what do we really know? Nat. Rev. Neurol. 7, 603–615.

Anderson, K.D., Gunawan, A., Steward, O., 2007. Spinal pathways involved in the control of forelimb motor function in rats. Exp. Neurol. 206, 318–331.

Antal, M., Freund, T.F., Polgar, E., 1990. Calcium-binding proteins, parvalbumin- and calbindin-D 28k-immunoreactive neurons in the rat spinal cord and dorsal root ganglia: a light and electron microscopic study. J. Comp. Neurol. 295, 467–484.

Azim, E., Jiang, J., Alstermark, B., Jessell, T.M., 2014. Skilled reaching relies on a V2a propriospinal internal copy circuit. Nature 508, 357–363.

Bareyre, F.M., Kerschensteiner, M., Raineteau, O., Mettenleiter, T.C., Weinmann, O., Schwab, M.E., 2004. The injured spinal cord spontaneously forms a new intraspinal circuit in adult rats. Nat. Neurosci. 7, 269–277.

Barriere, G., Mellen, N., Cazalets, J.R., 2004. Neuromodulation of the locomotor network by dopamine in the isolated spinal cord of newborn rat. Eur. J. Neurosci. 19, 1325–1335.

Belhaj-Saif, A., Cheney, P.D., 2000. Plasticity in the distribution of the red nucleus output to forearm muscles after unilateral lesions of the pyramidal tract. J. Neurophysiol. 83, 3147–3153.

Bjursten, L.M., Norrsell, K., Norrsell, U., 1976. Behavioural repertory of cats without cerebral cortex from infancy. Exp. Brain Res. 25, 115–130.

Chakrabarty, S., Shulman, B., Martin, J.H., 2009. Activity-dependent codevelopment of the corticospinal system and target interneurons in the cervical spinal cord. J. Neurosci. 29, 8816–8827.

Cheney, P.D., Fetz, E.E., Mewes, K., 1991. Neural mechanisms underlying corticospinal and rubrospinal control of limb movements. Prog. Brain Res. 87, 213–252.

Clemens, S., Belin-Rauscent, A., Simmers, J., Combes, D., 2012. Opposing modulatory effects of D1- and D2-like receptor activation on a spinal central pattern generator. J. Neurophysiol. 107, 2250–2259.

Cohen, N.R., Taylor, J.S., Scott, L.B., Guillery, R.W., Soriano, P., Furley, A.J., 1998. Errors in corticospinal axon guidance in mice lacking the neural cell adhesion molecule L1. Curr. Biol. 8, 26–33.

Cosottini, M., Giannelli, M., Siciliano, G., Lazzarotti, G., Michelassi, M.C., Del Corona, A., Bartolozzi, C., Murri, L., 2005. Diffusion-tensor MR imaging of corticospinal tract in amyotrophic lateral sclerosis and progressive muscular atrophy. Radiology 237, 258–264.

Courtine, G., Gerasimenko, Y., van den Brand, R., Yew, A., Musienko, P., Zhong, H., Song, B., Ao, Y., Ichiyama, R.M., Lavrov, I., Roy, R.R., Sofroniew, M.V., Edgerton, V.R., 2009. Transformation of nonfunctional spinal circuits into functional states after the loss of brain input. Nat. Neurosci. 12, 1333–1342.

Cowley, K.C., Zaporozhets, E., Schmidt, B.J., 2010. Propriospinal transmission of the locomotor command signal in the neonatal rat. Ann. N. Y. Acad. Sci. 1198, 42–53.

de Carvalho, M., Pinto, S., Swash, M., 2011. Does the motor cortex influence denervation in ALS? EMG studies of muscles with both contralateral and bilateral corticospinal innervation. Clin. Neurophysiol. 122, 629–635.

Deng, L.X., Deng, P., Ruan, Y., Xu, Z.C., Liu, N.K., Wen, X., Smith, G.M., Xu, X.M., 2013. A novel growth-promoting pathway formed by GDNF-overexpressing Schwann cells promotes propriospinal axonal regeneration, synapse formation, and partial recovery of function after spinal cord injury. J. Neurosci. 33, 5655–5667.

Ding, Y., Qu, Y., Feng, J., Wang, M., Han, Q., So, K.F., Wu, W., Zhou, L., 2014. Functional motor recovery from motoneuron axotomy is compromised in mice with defective corticospinal projections. PLoS ONE 9, e101918.

Feng, G., Mellor, R.H., Bernstein, M., Keller-Peck, C., Nguyen, Q.T., Wallace, M., Nerbonne, J.M., Lichtman, J.W., Sanes, J.R., 2000. Imaging neuronal subsets in transgenic mice expressing multiple spectral variants of GFP. Neuron 28, 41–51.

Feng, J., Xu, Y., Wang, M., Ruan, Y., So, K.F., Tissir, F., Goffinet, A., Zhou, L., 2012. A role for atypical cadherin Celsr3 in hippocampal maturation and connectivity. J. Neurosci. 32, 13729–13743.

Ferguson, T.A., Elman, L.B., 2007. Clinical presentation and diagnosis of amyotrophic lateral sclerosis. NeuroRehabilitation 22, 409–416.

Flynn, J.R., Graham, B.A., Galea, M.P., Callister, R.J., 2011. The role of propriospinal interneurons in recovery from spinal cord injury. Neuropharmacology 60, 809–822.

Greig, L.C., Woodworth, M.B., Galazo, M.J., Padmanabhan, H., Macklis, J.D., 2013. Molecular logic of neocortical projection neuron specification, development and diversity. Nat. Rev. Neurosci. 14, 755–769.

Han, P., Nakanishi, S.T., Tran, M.A., Whelan, P.J., 2007. Dopaminergic modulation of spinal neuronal excitability. J. Neurosci. 27, 13192–13204.

Han, Q., Feng, J., Qu, Y., Ding, Y., Wang, M., So, K.F., Wu, W., Zhou, L., 2013. Spinal cord maturation and locomotion in mice with an isolated cortex. Neuroscience 253, 235–244.

Harrison, P.J., Hultborn, H., Jankowska, E., Katz, R., Storai, B., Zytnicki, D., 1984. Labelling of interneurones by retrograde transsynaptic transport of horseradish peroxidase from motoneurones in rats and cats. Neurosci. Lett. 45, 15–19.

Harris-Warrick, R.M., Cohen, A.H., 1985. Serotonin modulates the central pattern generator for locomotion in the isolated lamprey spinal cord. J. Exp. Biol. 116, 27–46.

Irvine, K.A., Ferguson, A.R., Mitchell, K.D., Beattie, S.B., Beattie, M.S., Bresnahan, J.C., 2010. A novel method for assessing proximal and distal forelimb function in the rat: the Irvine, Beatties and Bresnahan (IBB) forelimb scale. J. Vis. Exp. (46), 1–9.

Jackson, C.E., Bryan, W.W., 1998. Amyotrophic lateral sclerosis. Semin. Neurol. 18, 27–39.

Jeffery, N.D., Fitzgerald, M., 2001. Effects of red nucleus ablation and exogenous neurotrophin-3 on corticospinal axon terminal distribution in the adult rat. Neuroscience 104, 513–521.

Jones, S.L., Light, A.R., 1992. Serotoninergic medullary raphespinal projection to the lumbar spinal cord in the rat: a retrograde immunohistochemical study. J. Comp. Neurol. 322, 599–610.

Jordan, L.M., Liu, J., Hedlund, P.B., Akay, T., Pearson, K.G., 2008. Descending command systems for the initiation of locomotion in mammals. Brain Res. Rev. 57, 183–191.

Kennedy, P.R., 1990. Corticospinal, rubrospinal and rubro-olivary projections: a unifying hypothesis. Trends Neurosci. 13, 474–479.

Kim, E.S., Li, H., McCulloch, P.F., Morrison, L.A., Yoon, K.W., Xu, X.M., 2000. Spatial and temporal patterns of transneuronal labeling in CNS neurons after injection of pseudorabies virus into the sciatic nerve of adult rats. Brain Res. 857, 41–55.

Kolb, B., Whishaw, I.Q., 1981. Decortication of rats in infancy or adulthood produced comparable functional losses on learned and species-typical behaviors. J. Comp. Physiol. Psychol. 95, 468–483.

Krageloh-Mann, I., Horber, V., 2007. The role of magnetic resonance imaging in elucidating the pathogenesis of cerebral palsy: a systematic review. Dev. Med. Child Neurol. 49, 144–151.

Lawrence, D.G., Kuypers, H.G., 1968. The functional organization of the motor system in the monkey. I. The effects of bilateral pyramidal lesions. Brain 91, 1–14.

Lemon, R.N., 2008. Descending pathways in motor control. Annu. Rev. Neurosci. 31, 195–218.

Liu, J., Jordan, L.M., 2005. Stimulation of the parapyramidal region of the neonatal rat brain stem produces locomotor-like activity involving spinal 5-HT7 and 5-HT2A receptors. J. Neurophysiol. 94, 1392–1404.

Liu, J.P., Baker, J., Perkins, A.S., Robertson, E.J., Efstratiadis, A., 1993. Mice carrying null mutations of the genes encoding insulin-like growth factor I (Igf-1) and type 1 IGF receptor (Igf1r). Cell 75, 59–72.

Liu, Y., Shi, J., Lu, C.C., Wang, Z.B., Lyuksyutova, A.I., Song, X.J., Zou, Y., 2005. Ryk-mediated Wnt repulsion regulates posterior-directed growth of corticospinal tract. Nat. Neurosci. 8, 1151–1159.

Liu, T.T., Bannatyne, B.A., Maxwell, D.J., 2010. Organization and neurochemical properties of intersegmental interneurons in the lumbar enlargement of the adult rat. Neuroscience 171, 461–484.

Muir, G.D., Whishaw, I.Q., 1999. Complete locomotor recovery following corticospinal tract lesions: measurement of ground reaction forces during overground locomotion in rats. Behav. Brain Res. 103, 45–53.

Musienko, P., van den Brand, R., Marzendorfer, O., Roy, R.R., Gerasimenko, Y., Edgerton, V.R., Courtine, G., 2011. Controlling specific locomotor behaviors through multidimensional monoaminergic modulation of spinal circuitries. J. Neurosci. 31, 9264–9278.

Nishimura, Y., Isa, T., 2012. Cortical and subcortical compensatory mechanisms after spinal cord injury in monkeys. Exp. Neurol. 235, 152–161.

Ozdinler, P.H., Macklis, J.D., 2006. IGF-I specifically enhances axon outgrowth of corticospinal motor neurons. Nat. Neurosci. 9, 1371–1381.

Qu, S., Ondo, W.G., Zhang, X., Xie, W.J., Pan, T.H., Le, W.D., 2006. Projections of diencephalic dopamine neurons into the spinal cord in mice. Exp. Brain Res. 168, 152–156.

Raineteau, O., Schwab, M.E., 2001. Plasticity of motor systems after incomplete spinal cord injury. Nat. Rev. Neurosci. 2, 263–273.

Raineteau, O., Fouad, K., Noth, P., Thallmair, M., Schwab, M.E., 2001. Functional switch between motor tracts in the presence of the mAb IN-1 in the adult rat. Proc. Natl. Acad. Sci. U. S. A. 98, 6929–6934.

Ren, K., Ruda, M.A., 1994. A comparative study of the calcium-binding proteins calbindin-D28K, calretinin, calmodulin and parvalbumin in the rat spinal cord. Brain research. Brain Res. Rev. 19, 163–179.

Riddle, C.N., Baker, S.N., 2010. Convergence of pyramidal and medial brain stem descending pathways onto macaque cervical spinal interneurons. J. Neurophysiol. 103, 2821–2832.

Rosenzweig, E.S., Courtine, G., Jindrich, D.L., Brock, J.H., Ferguson, A.R., Strand, S.C., Nout, Y.S., Roy, R.R., Miller, D.M., Beattie, M.S., Havton, L.A., Bresnahan, J.C., Edgerton, V.R., Tuszynski, M.H., 2010. Extensive spontaneous plasticity of corticospinal projections after primate spinal cord injury. Nat. Neurosci. 13, 1505–1510.

Schieber, M.H., 2007. Chapter 2. Comparative anatomy and physiology of the corticospinal system. Handb. Clin. Neurol. 82, 15–37.

Schmidt, B.J., Jordan, L.M., 2000. The role of serotonin in reflex modulation and locomotor rhythm production in the mammalian spinal cord. Brain Res. Bull. 53, 689–710.

Skagerberg, G., Lindvall, O., 1985. Organization of diencephalic dopamine neurones projecting to the spinal cord in the rat. Brain Res. 342, 340–351.

Smeraski, C.A., Sollars, P.J., Ogilvie, M.D., Enquist, L.W., Pickard, G.E., 2004. Suprachiasmatic nucleus input to autonomic circuits identified by retrograde transsynaptic transport of pseudorabies virus from the eye. J. Comp. Neurol. 471, 298–313.

Soteropoulos, D.S., Williams, E.R., Baker, S.N., 2012. Cells in the monkey ponto-medullary reticular formation modulate their activity with slow finger movements. J. Physiol. 590, 4011–4027.

Starkey, M.L., Barritt, A.W., Yip, P.K., Davies, M., Hamers, F.P., McMahon, S.B., Bradbury, E.J., 2005. Assessing behavioural function following a pyramidotomy lesion of the corticospinal tract in adult mice. Exp. Neurol. 195, 524–539.

Stelzner, D.J., Ershler, W.B., Weber, E.D., 1975. Effects of spinal transection in neonatal and weanling rats: survival of function. Exp. Neurol. 46, 156–177.

Terashima, T., 1995. Anatomy, development and lesion-induced plasticity of rodent corticospinal tract. Neurosci. Res. 22, 139–161.

Thuret, S., Moon, L.D., Gage, F.H., 2006. Therapeutic interventions after spinal cord injury. Nat. Rev. Neurosci. 7, 628–643.

Tillakaratne, N.J., Guu, J.J., de Leon, R.D., Bigbee, A.J., London, N.J., Zhong, H., Ziegler, M.D., Joynes, R.L., Roy, R.R., Edgerton, V.R., 2010. Functional recovery of stepping in rats after a complete neonatal spinal cord transection is not due to regrowth across the lesion site. Neuroscience 166, 23–33.

Tissir, F., Goffinet, A.M., 2013. Shaping the nervous system: role of the core planar cell polarity genes. Nat. Rev. Neurosci. 14, 525–535.

Tissir, F., Bar, I., Jossin, Y., De Backer, O., Goffinet, A.M., 2005. Protocadherin Celsr3 is crucial in axonal tract development. Nat. Neurosci. 8, 451–457.

Ueno, M., Hayano, Y., Nakagawa, H., Yamashita, T., 2012. Intraspinal rewiring of the corticospinal tract requires target-derived brain-derived neurotrophic factor and compensates lost function after brain injury. Brain 135, 1253–1267.

Umeda, T., Takahashi, M., Isa, K., Isa, T., 2010. Formation of descending pathways mediating cortical command to forelimb motoneurons in neonatally hemidecorticated rats. J. Neurophysiol. 104, 1707–1716.

Wilson, J.M., Blagovechtchenski, E., Brownstone, R.M., 2010. Genetically defined inhibitory neurons in the mouse spinal cord dorsal horn: a possible source of rhythmic inhibition of motoneurons during fictive locomotion. J. Neurosci. 30, 1137–1148.

Woodward, L.J., Anderson, P.J., Austin, N.C., Howard, K., Inder, T.E., 2006. Neonatal MRI to predict neurodevelopmental outcomes in preterm infants. N. Engl. J. Med. 355, 685–694.

Yeo, S.S., Jang, S.H., 2010. Changes in red nucleus after pyramidal tract injury in patients with cerebral infarct. NeuroRehabilitation 27, 373–377.

Yoshida, S., Hayakawa, K., Yamamoto, A., Okano, S., Kanda, T., Yamori, Y., Yoshida, N., Hirota, H., 2010. Quantitative diffusion tensor tractography of the motor and sensory tract in children with cerebral palsy. Dev. Med. Child Neurol. 52, 935–940.

Zaaimi, B., Edgley, S.A., Soteropoulos, D.S., Baker, S.N., 2012. Changes in descending motor pathway connectivity after corticospinal tract lesion in macaque monkey. Brain 135, 2277–2289.

Zhou, L., Bar, I., Achouri, Y., Campbell, K., De Backer, O., Hebert, J.M., Jones, K., Kessaris, N., de Rouvroit, C.L., O'Leary, D., Richardson, W.D., Goffinet, A.M., Tissir, F., 2008. Early forebrain wiring: genetic dissection using conditional Celsr3 mutant mice. Science 320, 946–949.